Global plasmasphere evolution 22–23 April 2001

J. Goldstein,[1] B. R. Sandel,[2] W. T. Forrester,[2] M. F. Thomsen,[3] and M. R. Hairston[4]

Received 21 June 2005; revised 24 August 2005; accepted 5 October 2005; published 20 December 2005.

[1] The evolution of the plasmasphere during the moderate 22–23 April 2001 storm is studied by comparing observed plasmasphere behavior to the predictions of a simulation. The plasmasphere observations include global images from IMAGE EUV and density and flow measurements from LANL MPA. The subjective uncertainty in the EUV plasmapause was found to be 0.2*L*. Inward plasmapause motion was correlated with southward interplanetary magnetic field (IMF), with a 27 min delay. The electric (E) field at the plasmapause was approximately 13% of the solar wind E-field. The observations support the idea that plasmaspheric erosion begins with a partial plasmapause indentation which then gradually widens in magnetic local time (MLT) to encompass the entire nightside. In situ measurements confirm a dayside plume of sunward flowing plasma, and images show that the plume subsequently experienced phases of MLT narrowing and rotation/wrapping. To simulate the event, we employed a test particle representation of the plasmapause using a parametric E-field model that includes corotation and convection from two sources: dayside magnetopause reconnection (DMR) and the subauroral polarization stream (SAPS). The model captures the phases of plume evolution, and it reproduces the observed plasmapause with maximum (mean) error <0.7*L* (0.24*L*). The model fails to reproduce important subglobal features (e.g., a predawn plasmaspheric shoulder) and grossly misplaces the inner edge of the rotating and wrapping plume. SAPS contributes significantly to the duskside flows, but the simulated flows are about 50% smaller than those seen by LANL MPA. The simulated plasmapause E-field is about 70% of the EUV-inferred value.

Citation: Goldstein, J., B. R. Sandel, W. T. Forrester, M. F. Thomsen, and M. R. Hairston (2005), Global plasmasphere evolution 22–23 April 2001, *J. Geophys. Res.*, *110*, A12218, doi:10.1029/2005JA011282.

1. Introduction

[2] Four decades of research have been devoted to studying the dynamics of the plasmasphere, the cold, dense, rotating torus of plasma that surrounds the Earth and forms the innermost part of the magnetosphere [*Lemaire and Gringauz*, 1998]. The plasmasphere is populated by the escape of ionospheric plasma which slowly (over the course of several hours or days) fills magnetic flux tubes. During geomagnetic disturbances the plasmasphere experiences erosion of its outer layers, in which the outer boundary (the plasmapause) generally moves inward on a timescale of a few hours. Thus at any given time the plasmasphere configuration results from its particular history of ionospheric filling and erosion [*Carpenter and Lemaire*, 1997].

[3] Plasmaspheric erosion is strongly correlated with intervals of southward interplanetary magnetic field (IMF) [*Carpenter et al.*, 1993; *Carpenter*, 1995; *Elphic et al.*, 1996; *Carpenter and Lemaire*, 1997; *Goldstein et al.*, 2003a]. It is generally accepted that southward IMF at the magnetopause leads to dayside magnetopause reconnection (DMR), driving sunward convection in the inner magnetosphere [*Dungey*, 1961], and that this sunward convection erodes the outer portion of the rotating plasmasphere. One byproduct of erosion is the plume, an elongated structure that extends outward from the main plasmasphere and into the outer magnetosphere. During erosion, plumes are most often found on the dayside, in the noon-to-dusk sector. The shape and location in magnetic local time (MLT) of a given plume can be described in terms of phases that follow the rise and fall of convection strength [*Goldstein and Sandel*, 2005]. At the onset of erosion resulting from increased convection, the plume is broadest in MLT extent, often filling much (or most) of the dayside inner magnetosphere. Intervals of prolonged convection cause the MLT extent of a preexisting plume to decrease; more mature plumes are narrower in MLT. When convection tapers off, the plume begins to rotate with the main plasmasphere, often becoming wrapped around it. These phases of plume formation and evolution have been identified in both single-point (in situ) measurements [*Chen et al.*, 1975; *Higel and Wu*, 1984;

[1]Space Science and Engineering Division, Southwest Research Institute, San Antonio, Texas, USA.
[2]Lunar and Planetary Laboratory, University of Arizona, Tucson, Arizona, USA.
[3]Space and Atmospheric Sciences Group, Los Alamos National Laboratory, Los Alamos, New Mexico, USA.
[4]Center for Space Sciences, University of Texas at Dallas, Richardson, Texas, USA.

0148-0227/05/2005JA011282$09.00

Moldwin et al., 1994; *Elphic et al.*, 1996; *Weiss et al.*, 1997] and global plasmasphere images [*Spasojević et al.*, 2003; *Sandel et al.*, 2001; *Goldstein et al.*, 2004b].

[4] The details of the erosion process are not completely understood, but some observations suggest that erosion begins with a partial indentation of the plasmapause which subsequently widens in MLT as the erosion progresses [*Carpenter and Lemaire*, 1997; *Goldstein et al.*, 2004c; *Goldstein and Sandel*, 2005]. It is unclear whether this widening indentation arises from plasmapause surface waves or is the plasmaspheric signature of a convective front propagating sunward at a finite speed [*Goldstein et al.*, 2005b]. Possibly related to a finite propagation speed of sunward convection, in every event (identified so far) for which reasonably precise timing is available, there is a 10–30-min delay between the arrival of southward IMF at the magnetopause and the subsequent onset of plasmaspheric erosion on the nightside [*Goldstein et al.*, 2003a; *Goldstein and Sandel*, 2005].

[5] Models that incorporate sunward convection in terms of a global dawn-to-dusk electric (E) field have been fairly successful at reproducing plasmaspheric erosion and the phases of plume evolution [*Grebowsky*, 1970; *Chen and Wolf*, 1972; *Spiro et al.*, 1981; *Lambour et al.*, 1997; *Goldstein and Sandel*, 2005]. However, a proper inner magnetospheric E-field model must include not just the global E-field imposed by the solar wind but also the important contributions from subglobal effects. It is known that electrodynamic coupling between the ring current and ionosphere can significantly modify the convection E-field. Ionospheric closure of region 2 field-aligned currents (FACs) can produce inner magnetospheric shielding [*Jaggi and Wolf*, 1973] and a duskside flow intensification known as the subauroral polarization stream (SAPS) [*Burke et al.*, 1998; *Foster and Burke*, 2002]. The contribution of neutral-wind/ionosphere coupling to the E-field experienced by the plasmasphere has also recently drawn attention [*Burch et al.*, 2004].

[6] Self-consistent simulations [e.g., *Spiro et al.*, 1981; *Fok et al.*, 2001; *Liemohn et al.*, 2004] should in principle provide the most accurate model electric fields, but because these simulations are often computationally expensive, it is also useful to have reasonably accurate parametric (analytical) representations of the inner magnetospheric E-field. Testing parametric convection E-field models via comparison with plasmasphere imaging has confirmed our zero-order understanding of global solar wind driven convection [*Goldstein and Sandel*, 2005], has improved our knowledge of the plasmaspheric effects of subglobal contributions such as shielding [*Goldstein et al.*, 2002] and SAPS [*Goldstein et al.*, 2003b], and has revealed new plasmaspheric features that require explanation [*Sandel et al.*, 2001; *Spasojević et al.*, 2003].

[7] In this paper we study plasmasphere evolution as affected by convection during and after a moderate storm that began on 22 April 2001. We compare the observed behavior of the plasmasphere to that predicted by a simulation that uses a solar wind and *Kp*-driven parametric E-field model to evolve a test-particle representation of the plasmapause. We show that the global-scale dynamic behavior of the plasmapause may be quantitatively reproduced via the use of a parametric potential electric field model that includes a newer parameterization of the SAPS effect [*Goldstein et al.*, 2005a]. This study adds to existing evidence [e.g., *Goldstein and Sandel*, 2005, and references therein] that certain subglobal phenomena (such as finite-MLT-width indentations and shoulder-like bulges) are probably general features of plasmaspheric dynamics that arise as a consequence of a temporally varying imbalance between convection and inner magnetospheric shielding. The 22 April 2001 storm presents additional evidence of a time delay between the onset of dayside magnetopause reconnection and the onset of nightside plasmaspheric erosion. A byproduct of this study is the quantification of the subjective error in plasmapause location determined from global imaging techniques.

2. Storm Event 22–23 April 2001

[8] On 22 April 2001 the magnetosphere experienced a moderate geomagnetic storm driven by a magnetic cloud. An overview of the event is shown in Figure 1. Coincident with a peak *Kp* value of 6^+ (see Figure 1a), the *Dst* index (Figure 1b) reached a minimum value of -102 nT at 1500 UT on 22 April, and the main phase of the storm lasted well into the following day. Solar wind and interplanetary magnetic field (IMF) conditions recorded by the Advanced Composition Explorer (ACE) [*Stone et al.*, 1998] are shown in Figure 1c through Figure 1f. All ACE data have been time-delayed by 63 min to account for propagation to the magnetopause, using a simple distance ÷ speed approximation. Plasma density (Figure 1c) was low to moderate (roughly between 5 and 15 cm^{-3}) and solar wind speed V_{SW} (Figure 1d) fell gradually from 390 km/s to 300 km/s during 22–23 April. The IMF component parallel to the geomagnetic field ($B_{z,IMF}$ in Figure 1e) was southward for three distinct intervals on 22 April (labeled "1," "2," and "3" in Figure 1e): 0130–0200 UT, 0217–0430 UT, and after 0434 UT. Starting at 0900 UT on 22 April, the IMF (Figures 1e and 1f) exhibited a magnetic cloud signature (a smooth, gradual rotation of the magnetic field direction), during which $B_{z,IMF}$ remained southward. Southward IMF presumably imposes on the inner magnetosphere a globally dawn-to-dusk electric field that drives sunward convection, leading to plasmasphere erosion, as discussed in the next section.

3. Plasmasphere Observations

[9] The extreme ultraviolet (EUV) imager on board the Imager for Magnetopause-to-Aurora Global Exploration (IMAGE) satellite obtains global images of the helium portion of the plasmasphere [*Sandel et al.*, 2001] by capturing 30.4-nm sunlight resonantly scattered by He^+ ions (which comprise 5–10% of the total ion population). The EUV instrument is composed of three cameras with slightly overlapping fields of view. The EUV imager observes the high-density portion of the plasmasphere, with a nominally lower sensitivity threshold equivalent to total ion density of 40 cm^{-3} [*Goldstein et al.*, 2003c]. Extraction of the plasmapause boundary [*Roelof and Skinner*, 2000] from a sequence of EUV images provides a series of global snapshots of the equatorial plasmapause, with temporal and nominal spatial resolution of 10 min and 0.1 R_E [*Sandel et*

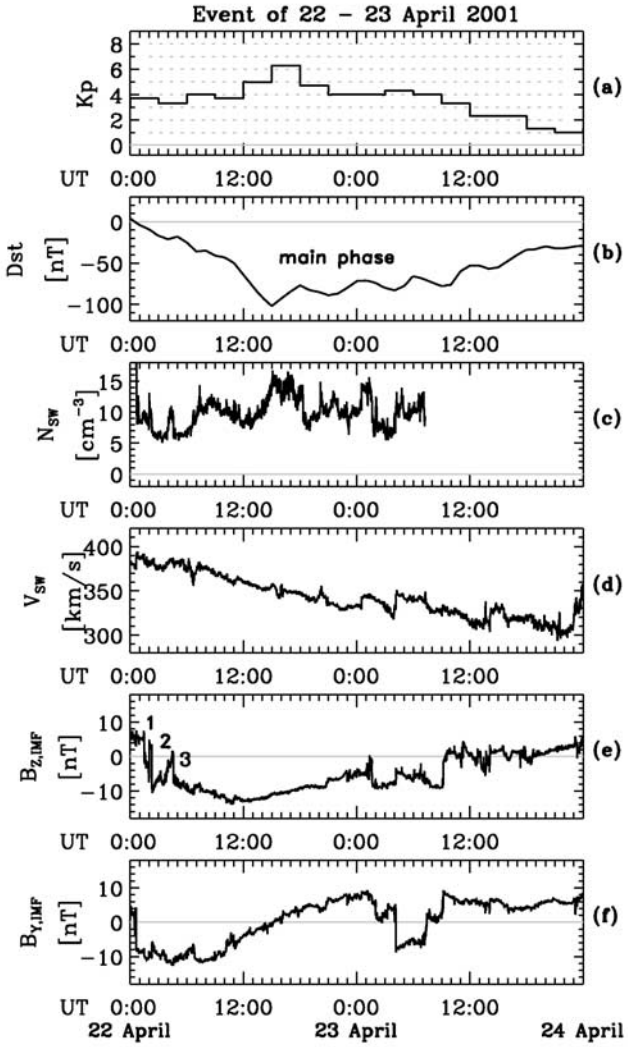

Figure 1. Summary/overview of 22–23 April 2001 storm event. (a) *Kp* midlatitude 3-hour geomagnetic disturbance index. Peak value (during 1500–1800 UT on 22 April) was $Kp = 6^{+}$. (b) *Dst* low-latitude 1-hour disturbance index. At the peak of the storm (1500 UT) $Dst = -102$ nT (moderate storm). (c and d) Solar wind number density and speed measured upstream by ACE SWEPAM. Note data dropout in density after 0700 UT on 23 April. (e and f) Interplanetary magnetic field (IMF) *Z*- and *Y*-components (GSM coordinates) measured by ACE MAG. The smooth, gradual rotation of strong magnetic field is a typical magnetic cloud signature.

al., 2001; *Goldstein et al.*, 2003c]. Lacking a robust automated technique, EUV plasmapause extraction is done manually. As discussed in section 6, the estimated subjective error in the extracted EUV boundaries of 22 April 2001 is 0.2*L*.

[10] The 22–23 April 2001 IMAGE EUV plasmapause observations are presented in Figure 2. A dozen plasmapause snapshots are plotted in Figures 2a through 2l, and a summary plot is given in Figure 2m, as described in the caption. Five phases of the event are indicated by the text labels accompanying groups of snapshots whose plasmapause points are all the same color (e.g., all the red points in Figures 2b through 2f go with the label "Erosion Onset"). Most of the plasmapause snapshots contain no data in the range 1200–2100 MLT because throughout the event, the camera whose field of view covered the duskside was usually turned off to prevent sunlight from entering the camera, producing a gap in the duskside plasmasphere images.

3.1. Initial Plasmasphere, 22 April

[11] Before 0250 UT on 22 April, the nightside plasmasphere had no sharp outer density gradient, as reflected by the diffuse/scattered band of points west of 0600 MLT in the 0240 UT snapshot of Figure 2a. A gradual outer density gradient is typically seen in EUV images after prolonged periods of low-to-moderate geomagnetic activity [*Spasojević et al.*, 2003], during which ionospheric outflow gradually fills plasmaspheric flux tubes. At 0240 UT the outermost boundary of plasmaspheric plasma visible to EUV was at $L \approx 5$ on the nightside and $L \approx 4–5$ on the dayside. This type of diffuse outer boundary often reflects not the actual plasmapause but the location where a gradually decreasing density-versus-*L* profile crosses below the EUV sensitivity threshold [*Goldstein et al.*, 2003c]. Consistent with this, geosynchronous observations before 0524 UT (see Figure 3) show ion number densities all below about 11 cm^{-3} and roughly 2 cm^{-3} on average.

3.2. Nightside Erosion Onset, 22 April

[12] At about 0250 UT the erosion began ("Erosion Onset" in Figure 2) with a partial plasmapause indentation which subsequently widened in MLT. The EUV outer boundary between 0100–0300 MLT began moving inward, forming an indentation. Unlike the initial boundary of Figure 2a, the indented boundary was well-defined, indicating a steep plasmapause density gradient [*Goldstein et al.*, 2003c]. Over the next 2 UT hours (Figures 2b–2f), the indentation widened in MLT, and within the MLT range of the widening indentation, the formerly diffuse outer boundary was transformed to a steep outer density gradient with a smoother MLT-shape. The MLT-edges of the widening indentation were marked by ripples, i.e., transitions from reduced plasmapause *L* and steep outer density gradient (the indentation) to the diffuse, large *L* outer boundary of the initial plasmapause. For example, the eastern ripple moved from about 0500 MLT (Figure 2b) to 0600 MLT (Figure 2d) between 0331 and 0412 UT. MHD-based models and particle models (such as the Rice Convection Model) suggest that inward plasmapause motion results from both inward (compressional) and azimuthal (erosional) plasma motion (see *Spiro et al.* [1981], *Goldstein and Sandel* [2005], and section 7). With the understanding that eastward corotation should add to (subtract from) the sunward directed convection on the dawnside (duskside), one might expect that the eastward moving ripple (at the eastern edge of the widening indentation) would move faster than the westward moving ripple. There is no discernible difference in the speed of the eastward moving and westward moving ripples of 22 April, perhaps in part because of the duskside

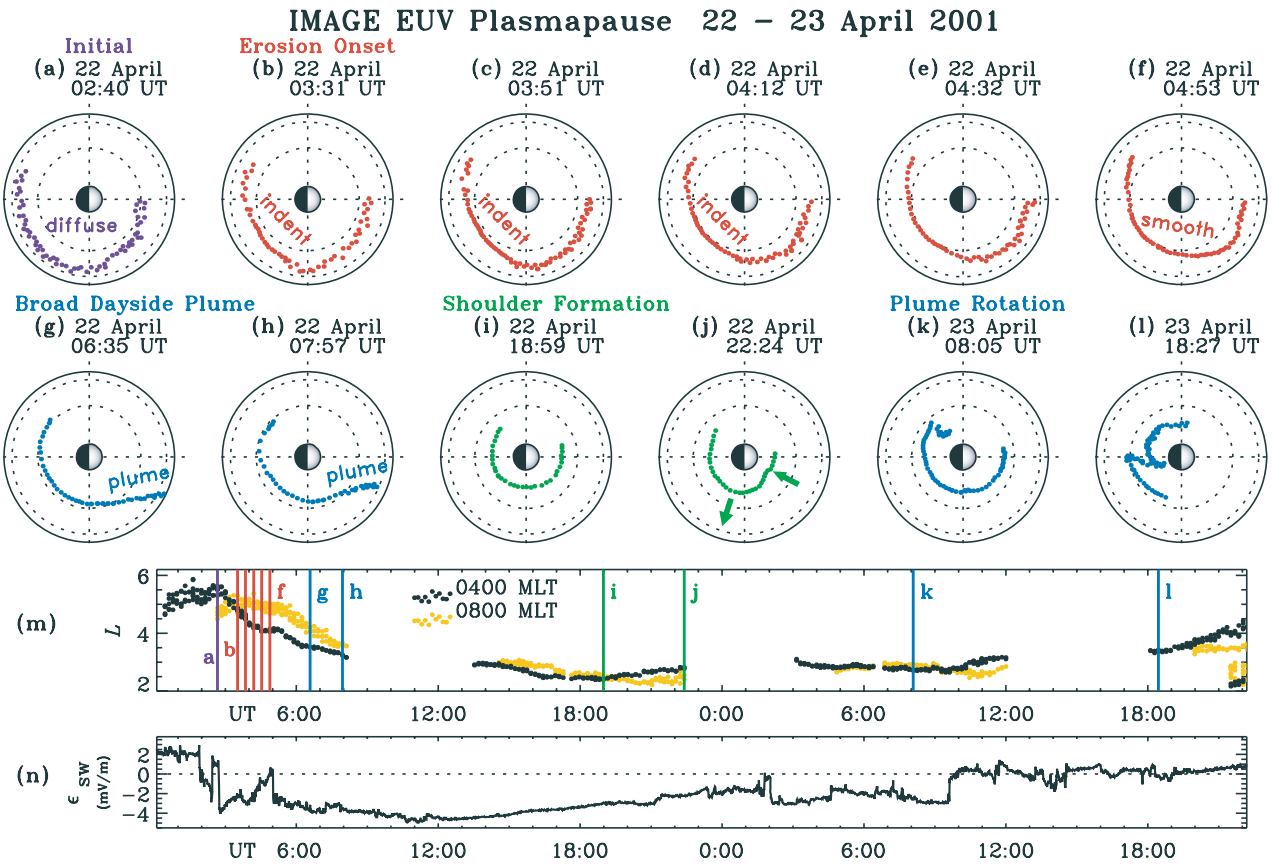

Figure 2. (a through l) Global plasmapause snapshots obtained from the IMAGE EUV imager. In each plot, the view is of the SM-coordinate magnetic equatorial plane, with the Sun to the right and the Earth in the center. Circles are drawn at $L = 4$, 6 (dotted lines), and $L = 6.62$ (solid line). The manually extracted plasmapause points are dots, color-coded to match accompanying phases of the event ("Initial," "Erosion Onset," "Broad Dayside Plume," "Shoulder Formation," and "Plume Rotation"), as described in the text. (m) Summary of EUV plasmapause observations showing plasmapause L value from two 1-hour MLT bins centered at 0400 MLT (black) and 0800 MLT (yellow-orange). Color-coded vertical lines mark the times of the individual snapshots a through l. (n) Dusk-to-dawn solar wind electric field $\epsilon_{SW} \equiv V_{SW}B_{z,IMF}$, delayed 27 min beyond the magnetopause; note that negative ϵ_{SW} means southward $B_{z,IMF}$ and a dawn-to-dusk E-field.

gap in EUV coverage (which prevents reliable determination of the speed of the westward moving ripple). However, in other events, the eastward moving ripple typically moves slightly faster despite the presence of duskside flow enhancement by the SAPS effect [*Goldstein et al.*, 2004c, 2005b; *Goldstein and Sandel*, 2005]. Comparing Figures 2a and 2f shows that the net result of the initial 2 hours of the erosion was a reduction of the nightside plasmapause by about 1.5 to 2 R_E.

[13] The black dots in Figure 2m show the nightside plasmapause locations in a 1-hour-wide bin centered at 0400 MLT (i.e., 0330–0430 MLT), plotted versus time. Shortly after 0240 UT (purple line labeled "a"), the 0400 MLT plasmapause L value dropped steeply. Throughout much of the rest of the day, the nightside plasmapause continued to move inward, and the inward motion was in phase with intervals during which the inner magnetosphere most likely experienced enhanced reconnection-driven convection. In Figure 2n is plotted the ACE-measured ϵ_{SW}, defined as the dusk-to-dawn E-field ($V_{SW}B_{z,IMF}$) imposed by the solar wind, which is negative for southward IMF (i.e., sunward convection). The best correlation between negative ϵ_{SW} intervals and nightside plasmaspheric erosion on 22 April occurs if in addition to the 63 min propagation delay to bring the ACE measurements to the magnetopause, an additional 27 min delay is added. This 27 min delay

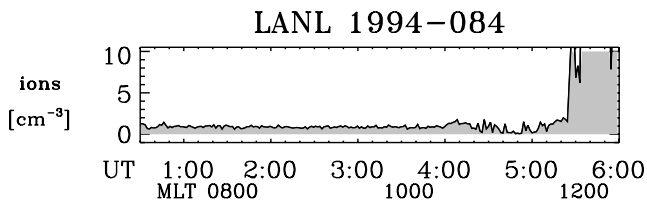

Figure 3. Ion number density measured by the MPA instrument on board geosynchronous satellite LANL 1994-084, 22 April 2001. Before 0524 UT (when a sunward moving plume crossed geosynchronous orbit), the average MPA-measured density was about 2 cm^{-3}.

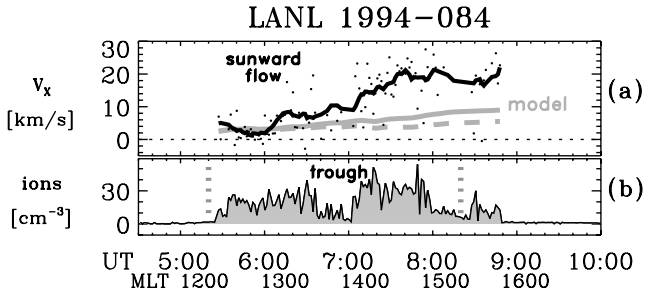

Figure 4. Measurements of the MPA instrument on board geosynchronous satellite LANL 1994-084, 22 April 2001. (a) Sunward (+*X*) component of inertial-frame plasma flow; dots are unfiltered data, thick black line is a 14-min boxcar average. The thick gray solid (dashed) line is a model with (without) SAPS flows included (see section 5). The plasma in the plume flowed sunward, with speed increasing toward duskside MLT. (b) Ion density profile, clearly indicating a dayside plume (density >10 cm^{-3}) between 1210 and 1540 MLT. The gray vertical dotted lines show the extent of the plume in the simulation, which roughly agrees with the observations (see text).

between the arrival of southward IMF at the magnetopause and the subsequent onset of erosion is consistent with previous EUV erosion timing studies [*Goldstein and Sandel*, 2005]. During intervals of negative (delayed) ϵ_{SW}, the nightside plasmapause generally moved inward; when ϵ_{SW} changed to positive (or zero) polarity, the plasmapause motion ceased, e.g., at about 0500 UT. Plasmapause inward motion also slowed down or ceased after a prolonged interval of roughly steady convection (e.g., about 1800 MLT), perhaps because a quasi-steady-state balance between convection and corotation had been established or because effective shielding developed [*Jaggi and Wolf*, 1973; *Kelley et al.*, 1979].

3.3. Broad Dayside Plume, 22 April

[14] Interpretation of the dayside EUV data of 0240–0450 UT requires more care than the nightside. The diffuse dayside outer boundary probably represents the lower sensitivity threshold (LST) and not an actual plasmapause density gradient. Unlike the nightside where sunward convection moved plasma inward (steepening the density gradient), on the dayside, convection moved plasma outward, blurring an already gradual density gradient. Despite this difficulty, available evidence from EUV images and in situ data indicates that while the nightside plasmapause moved inward, the dayside plasma moved sunward to form a plume, and that this plume narrowed in MLT as the erosion event progressed. This evidence will now be presented.

[15] In the 0700–1200 MLT sector, the outermost EUV boundary moved outward slightly, from $L \approx 4.5$ to $L \approx 5$ during 0240–0331 UT (Figures 2a and 2b). The same story is told in Figure 2m; the yellow dots are the plasmapause locations in a 1-hour-wide bin centered at 0800 MLT. This initial motion (between 0240 and 0331 UT) probably indicates that denser plasma was moved to higher *L* values, shifting outward the location where the gradual density profile crossed the LST.

[16] Within the field of view (FOV) of the EUV images of 0635–0757 UT (Figures 2g and 2h) the dawnside portion of a broad plume can be seen extending sunward into the dayside magnetosphere. For example, in Figure 2g the plume's dawnside edge crosses geosynchronous orbit (6.62 R_E) at about 1024 MLT. Simultaneous in situ measurements from geosynchronous orbit confirm the presence of the dayside plume implied by the EUV images, as follows. Figure 4 contains ion density and flow information obtained during 0500–1000 UT on 22 April, in the afternoon sector (1200–1700 MLT) by the Magnetospheric Plasma Analyzer (MPA) instrument [*McComas et al.*, 1993] on board the Los Alamos National Laboratory (LANL) satellite 1994-084. At about 0524 UT and 1210 MLT, the satellite entered a dayside plume (density >10 cm^{-3}) whose MLT extent was approximately 3.5 MLT hours (Figure 4b). Consistent with a plume interpretation of the LANL (and EUV) data, the plasma flows in the same MLT range were directed sunward (Figure 4a). Figure 5 shows density and flows from two other geosynchronous platforms. LANL 1991-080 was in the dusk sector during the early phase of the erosion and observed a brief interval of low-density (well under 30 cm^{-3}; see Figure 5a) cold plasma, headed sunward (at about 10 km/s; see Figure 5b). This sunward moving low-density plasma was in the duskside gap in IMAGE EUV coverage (see discussion above) but most likely would have been difficult or impossible to see because its density was mostly well below the nominal EUV sensitivity threshold. Figures 5c and 5d show that LANL-01A passed through a sunward moving plume of plasma between 1100 and 1600 UT, with the densest part of the plume (above 25 cm^{-3}) observed during 1117–1440 UT. The LANL-01A observations during this time period bridge a gap in EUV coverage that occurred between 0807 and 1332 UT and are also consistent with the convection-driven plume hypothesis. The additional observations of Figure 5 provide

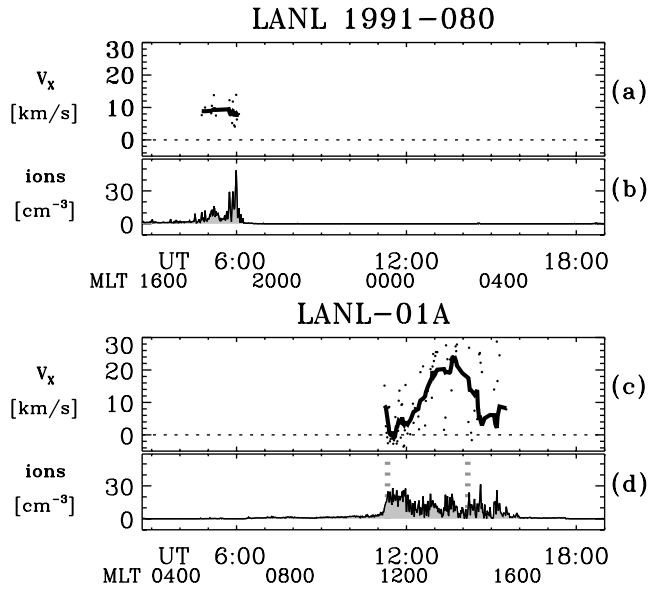

Figure 5. Measurements of the MPA instrument on board geosynchronous satellites LANL 1991-080 and LANL-01A, 22 April 2001. The format of each pair of plots follows that of Figures 4a and 4b.

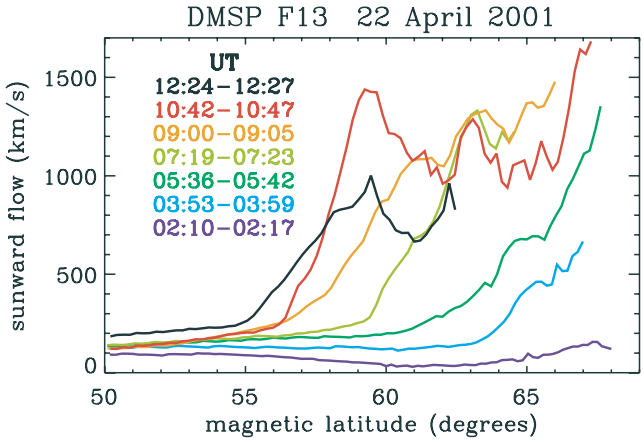

Figure 6. Drift meter measurements from the DMSP F13 satellite, in a roughly dawn-dusk orbit on 22 April 2001. Several passes through the duskside subauroral region are shown, color-coded by UT (as given in the legend). Sunward flows at subauroral latitudes increased dramatically after 0719 UT and then began decreasing after 1224 UT.

a slightly more complete picture of the erosion event and also confirm the presence of low-density plasma moving sunward, probably invisible to IMAGE EUV. As discussed in section 5.3.1, the LANL plume observations in Figure 4b and Figure 5d are in reasonable agreement with the simulation results to be presented later.

[17] In Figure 4a, sunward flow speeds observed by LANL 1994-084 inside the plume steeply increase with MLT. It is likely that SAPS was a major contributor to this duskside flow increase [*Goldstein et al.*, 2004b]. First, the average spatial distribution of SAPS contains a concentration of strong flows near dusk. Second, after about 0719 UT on 22 April 2001, the Defense Meteorological Satellite Program (DMSP) F13 satellite observed (in the ionosphere at about 840 km altitude) a dramatic increase in the strength of sunward flows at subauroral latitudes, from $\leq$100 km/s to over 1000 km/s (see Figure 6). Such strong sunward flows in the subauroral region are a well-known byproduct of the SAPS effect [*Foster and Vo*, 2002]. Crudely mapping the 1 km/s ionospheric SAPS flows to the magnetic equator via an $R^{3/2}$ dependence gives about 20 km/s, consistent with the duskside LANL-observed flows of Figure 4a. The SAPS effect started to decrease after 1224 UT (see Figure 6), consistent with the fact that LANL-01A observed reduced duskside flows (relative to those seen by LANL 1994-084) during its later pass through the plume (see Figure 5c). Thus a SAPS interpretation of the strong duskside flows is justifiable based on both the general spatial and specific temporal properties of the subauroral polarization stream. In section 5.3.2 we support this assertion with simulation output.

[18] The EUV observations during the several hours following the formation of the 22 April plume support the convective model prediction that during prolonged convection, a plume's MLT width gradually shrinks because the western edge migrates eastward [*Goldstein and Sandel*, 2005]. For example, in the 1 hour 22 min between 0635 UT (Figure 2g) and 0757 UT (Figure 2h), the L = 4 crossing of the plume edge moved eastward from 0800 MLT to 0915 MLT. The EUV boundary motion at 0800 MLT (yellow dots in Figure 2m) also illustrates the plume narrowing process. After about 0500 UT, the EUV boundary (yellow dots in Figure 2m) began moving inward; this occurred because by 0500 UT the eastern edge of the widening MLT indentation (see section 3.2) reached 0800 MLT. Thus the plume narrowing process, in which the western edge of the plume moves eastward, can be viewed as an aspect of the gradual process of widening of the initial MLT indentation that began the erosion. As mentioned in the last section, the rate of widening of the initial MLT indentation depends on contributions from both convection and corotation. Corotation certainly plays a strong role in the eastward transport of the western plume edge, whereas the westward widening of the indentation (on the nightside) may be more directly related to a propagating convection front (as discussed in section 1).

[19] Further plume narrowing was not directly observed because of a gap in EUV image coverage between 0807 and 1332 UT. After 1332 UT the EUV-observed dayside plasmapause was roughly circular (at $L \approx 2$–3), with a data gap (owing to sunlight contamination) roughly between 1200 and 2100 MLT. Numerous other EUV-observed plume events [*Spasojević et al.*, 2003; *Goldstein and Sandel*, 2005] and the plasmapause test particle simulation of this paper (to be discussed later) lend confidence to the assertion that plume narrowing did in fact occur on 22 April 2001 and that after 1332 UT the narrowed plume was located in the MLT coverage gap of the EUV images.

3.4. Shoulder Formation, 22 April

[20] Between 1859 and 2224 UT (Figures 2i and 2j), the predawn plasmapause moved outward while the post-dawn plasmapause moved inward. The net effect of these two motions was to form a mild shoulder-like predawn bulge of the plasmapause. Predawn plasmaspheric shoulders have been associated with overshielding of the inner magnetosphere following a convection decrease [*Goldstein et al.*, 2002, 2003d], and in accord with this, the mild shoulder of 22 April formed during a period of decreasing ϵ_{SW} magnitude (see Figure 2n). Theoretical studies suggest that overshielding creates a dawnside eddy flow pattern in which predawn plasma flows radially outward and postdawn plasma flows radially inward [*Senior and Blanc*, 1984; *Goldstein et al.*, 2002]; this is the flow pattern implied by the plasmapause motion during 1859–2224 UT on 22 April. The shoulder formation can be identified in Figure 2m: during the interval between the two green vertical lines ("i" and "j"), the 0400 MLT plasmapause L (black dots) increased while the 0800 MLT plasmapause L (yellow dots) decreased. A similar signature, following the sudden positive turning of ϵ_{SW} at 0930 UT on 23 April (1.5 hours after the blue vertical line "k") may also have been produced by overshielding. The predawn outward motion of the plasmapause after 1800 UT on 23 April was not a shoulder formation but rather was associated with the gradual eastward rotation of the plume, discussed next.

3.5. Plume Rotation, 23 April

[21] For most of the 22–23 April event (save for a few isolated snapshots on 23 April), the duskside plasmapause

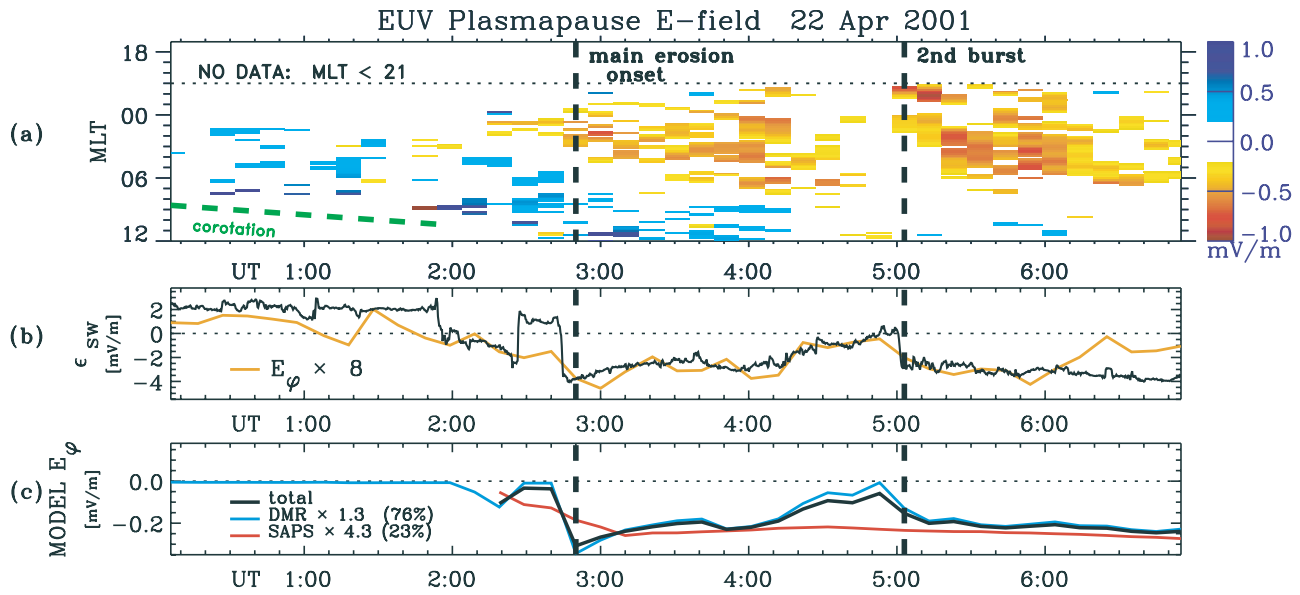

Figure 7. Plasmapause electric field E_π inferred from IMAGE EUV, 22 April 2001, during the first few hours of plasmasphere erosion. (a) E_π versus MLT and UT, color-coded according to the legend at the right. Red (blue) is inward (outward) radial motion at a fixed MLT. White is no data, or $|E_\pi| \leq 2$ mV/m. The green dashed line indicates motion following strict corotation with the Earth. Note that no plasmapause data were obtained for MLT < 2100 (i.e., above the horizontal dotted line) because of duskside sunlight contamination. (b) Dusk-to-dawn solar wind E-field ϵ_{SW} (black line) and plasmapause E-field (E_φ) × 8 in the range 0000–0300 MLT (orange line). On 22 April, the plasmapause E-field was about 13% of the solar wind E-field. (c) Model plasmapause E-field in the range 0000–0300 MLT. Black line: total E_φ. Blue line: scaled DMR contribution (DMR is ≈10% of ϵ_{SW}). Red line: scaled SAPS contribution (SAPS is ≈3% of ϵ_{SW}).

between 1200 and 2100 MLT was not captured by EUV (because of the aforementioned sunlight contamination). The MLT coverage gap precluded imaging observations that could verify an afternoon-sector plume during the plume narrowing stage of the erosion (after 0807 UT on 22 April), although LANL 1991-080 geosynchronous data (not shown) from 0130–0430 UT on 23 April do show an apparent plume of 20–60 cm^{-3} plasma between 1400 and 1700 MLT.

[22] On 23 April the average magnitude of the convection E-field (ϵ_{SW}) decreased (relative to 22 April), and the plume rotated eastward. At about 0805 UT on 23 April, the base of the plume rotated out of the MLT gap and was visible to EUV (Figure 2k). At 1827 UT (Figure 2l), 9 hours after a drastic reduction (to nearly 0 mV/m) in the magnitude of ϵ_{SW}, the eastward rotating plume was fully visible to EUV.

4. Plasmapause Electric Field

[23] To a very good degree of approximation, cold plasmaspheric plasma is subject only to $E \times B$ drift [*Spiro et al.*, 1981]. With this assumption, the motion of the plasmapause boundary provides some information about the local electric field [*Carpenter et al.*, 1972]. In general, it is possible to infer only E_π, defined as the component of the total E-field that is locally tangent to the plasmapause [*Goldstein et al.*, 2004c]. For a perfectly circular plasmapause, E_π reduces to the azimuthal component E_φ. Defining $\alpha(\varphi)$ as the angle between the local plasmapause tangent direction and the azimuthal unit vector, it is possible to estimate E_φ at MLT locations where α is small [*Goldstein et al.*, 2004c].

[24] The uncertainty in E_φ due to subjectivity in the plasmapause extraction is significant. Given a 0.2 L uncertainty in plasmapause L (see section 6), we estimate $\Delta E_\varphi \approx 66\ L^{-3}$ mV/m, where the L^{-3} factor comes from the dipole B assumed to convert plasmapause motion into an E-field. The uncertainty in E_φ increases as the eroding plasmpause moves inward, from $\Delta E_{L=6} \approx 0.4$ mV m^{-1} to $\Delta E_{L=4} \approx 1$ mV m^{-1}. The EUV-inferred plasmapause E-field of 22 April 2001 is displayed in Figure 7.

[25] Figure 7a shows a two-dimensional plot of E_φ, obtained from E_π for $\alpha \leq 9°$ (i.e., $\cos\alpha \geq 0.99$ or $E_\pi \approx E_\varphi$). Noting that inward plasmapause motion appears in Figure 7a as red-orange color (−0.2 to −1 mV/m), there were two main bursts of erosion, indicated with vertical dashed lines (and labels "main erosion onset" and "2nd burst"). For reference, Figure 7b (black line) plots the dusk-to-dawn solar wind E-field ϵ_{SW} (from Figure 2). It is clear that the erosion intervals are strongly correlated with intervals of negative ϵ_{SW} (i.e., southward IMF). Although the main erosion did not begin until 0250 UT, there was some inward plasmapause motion just east of midnight MLT that preceded the main erosion, perhaps resulting from the brief period of negative ϵ_{SW} during 0200–0225 UT.

[26] The E_φ plot in Figure 7a illustrates that the erosion process affected different MLTs at different times. Erosion began as a partial indentation (in a finite MLT range) which widened to encompass more of the plasmapause. As mentioned earlier, this type of indentation signature has

been seen in E-field analysis of other EUV-observed disturbance events [*Goldstein et al.*, 2004c, 2004a] and appears to be a consistent part of the global erosion process.

[27] Many models assume that only some fraction of the solar wind E-field is actually experienced by the inner magnetospheric plasma [e.g., *Maynard and Chen*, 1975]. The ratio of E_φ to ϵ_{SW} gives some indication of this fraction; close to midnight MLT, E_φ is parallel to $-Y$ (i.e., to ϵ_{SW}). In Figure 2b the average E_φ in the MLT range 0000–0300 MLT is compared to ϵ_{SW}. The magnitude of ϵ_{SW} is approximately 8 times that of E_φ, by itself implying 13% transfer of the solar wind E-field to the inner magnetosphere via dayside magnetopause reconnection (DMR). However, we note that DMR is not the only contributor to the plasmapause E-field, as shown by *Goldstein et al.* [2003b] and discussed in the next section.

5. Plasmapause Simulation

[28] To test the convection-based interpretation of the 22 April erosion event, we ran a very simple plasmapause test particle (PTP) simulation that has proven reasonably successful at reproducing observations [*Goldstein et al.*, 2003b, 2005a]. The PTP formulation represents the changing equatorial plasmapause as an arbitrary (large) number of cold test particles subject only to $E \times B$-drift in a time-varying convection E-field. Test particles are added or removed as necessary to resolve the plasmapause shape and maintain interparticle distance within the range 0.05–0.4 R_E. For this event the simulation was run with a 30-s time step.

5.1. Convection Electric Field

[29] We assume potential flow, ignoring induction electric fields. This limitation precludes treatment of the plasmaspheric effects of substorm dipolarization and magnetic inflation by ring current pressure enhancement. Dipolarization has been observed to produce an impulsive (temporary) distortion of the plasmapause boundary, and magnetic inflation may lead to an observable (1 R_E) outward bulge of the plasmapause in the MLT sector of the partial ring current (generally dusk-to-midnight for substorm injections) [*Goldstein et al.*, 2004a, 2005b]. Neither of these effects were specifically identifiable in the plasmasphere observations of 22 April 2001. The total electric field imposed on the test particles is the sum of a corotational (i.e., radially inward) E-field and a convection E-field that on a global scale points from dawn-to-dusk but includes spatial variation on subglobal scales. The convection E-field for the model is assumed to have two sources: a partially shielded DMR-driven part and a contribution from the subauroral polarization stream (SAPS).

5.1.1. DMR Contribution

[30] The DMR-driven contribution to convection is modeled by the shielded equatorial Volland-Stern electric potential [*Volland*, 1973; *Stern*, 1975]:

$$\Phi_{VS} = -A\, r^2 \sin\varphi, \tag{1}$$

where r and φ are the radial and azimuthal cylindrical coordinates in the SM equatorial plane. A uniform dawn-to-dusk convection electric field of magnitude E_0 would have the potential $\Phi_{uniform} = -E_0\ r\ \sin\varphi$. The Volland-Stern convection potential deals with shielding by setting the exponent of r to 2, which produces equipotentials that curve away from the Earth. This crude approximation ignores known azimuthal and temporal variations in the shielding strength [*Fejer and Scherliess*, 1995] and is inadequate to address overshielding, in which a residual dusk-to-dawn E-field remains after reduction of a strong convection E-field [*Jaggi and Wolf*, 1973]. In truth, the Volland-Stern potential is not entirely realistic at large r, but inside geosynchronous orbit it is a reasonable tool for studying the effect of DMR-driven convection [*Korth et al.*, 1999].

[31] In equation (1), A is a normalization constant taken to be

$$A = 0.10\, E_{SW}\, (6.62\, R_E)^{-1}, \tag{2}$$

following *Goldstein et al.* [2005a]. Here $E_{SW} \equiv |\epsilon_{SW}|$, with the constraint $E_{SW} \geq 0.1$ mV/m (to represent a finite viscous interaction with the solar wind during northward IMF). The normalization constant A is equivalent to 10% of the solar wind E-field applied inside geosynchronous orbit. From Figure 7b the magnitude of the total plasmapause E-field on 22 April 2001 was approximately 13% of the solar wind E-field. To account for the EUV-inferred E-field then requires a second E-field with magnitude equal to 3% of E_{SW}; in our model this contribution comes from SAPS (see sections 5.1.2 and 5.3.2).

5.1.2. SAPS Contribution

[32] In the magnetic equatorial plane, the subauroral polarization stream (SAPS) is a westward flow channel located at the inner edge of the ion ring current roughly in the dusk-to-midnight MLT sector. The SAPS effect has been demonstrated to play a crucial role in plasmaspheric dynamics; enhanced westward flows near dusk can move the plasmapause inward, smooth its MLT shape, and at times create distinct narrow duskside plumes [*Foster et al.*, 2002; *Goldstein et al.*, 2003b]. To include this effect, we use an equatorial SAPS model which approximates the radially narrow flow channel as a steep potential drop whose magnitude varies with time and MLT [*Goldstein et al.*, 2005a]. The equatorial SAPS potential is parameterized by *Kp* (in the range $4 \leq Kp \leq 7$), based on observed average SAPS properties [*Foster and Vo*, 2002]. A major limitation of the *Kp*-driven model is that it does not really capture the dynamic spatial and temporal properties of SAPS; e.g., the model approximates a brief interval of strong SAPS flows as a longer interval of weaker flows. The model cannot reliably predict the moment-to-moment SAPS strength at its precise location but provides an empirically based estimate for the average SAPS strength that can improve the performance of PTP simulations on the duskside [*Goldstein et al.*, 2003b, 2005a]. The output of the PTP simulation is shown in Figure 8, which is formatted similarly to Figure 2.

5.2. Initial Conditions

[33] The initial plasmapause for the simulation was specified using the IMAGE EUV outer boundary locations of Figure 2a, which are replotted (in the same format) in Figure 8a. In the simulation, the EUV L points of 0240 UT (22 April) were represented by a 200-point discretization of a

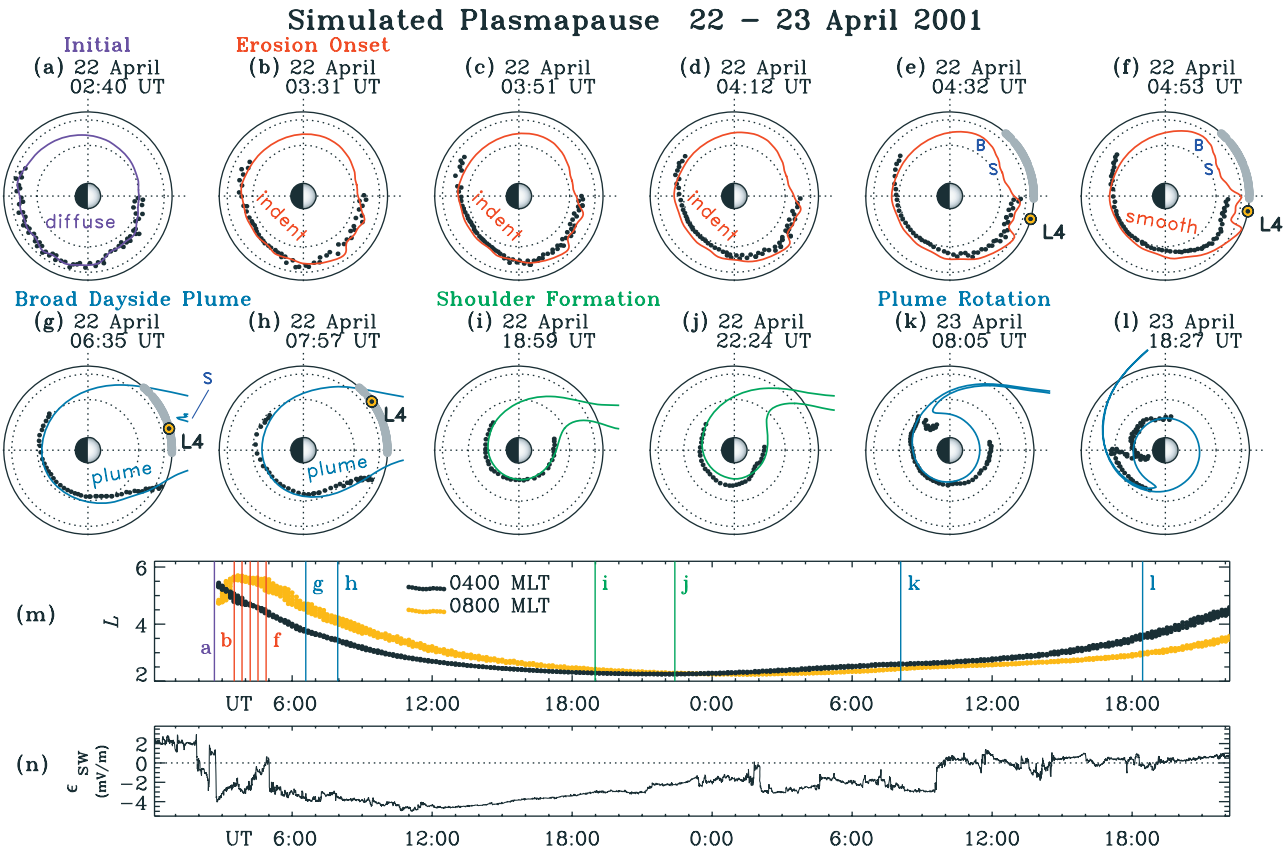

Figure 8. Results from the plasmapause test particle (PTP) simulation of the 22–23 April 2001 event. The model was driven by a time-varying convection E-field with contributions from the solar wind and the subauroral polarization stream (SAPS). The format of this figure is almost identical to that of Figure 2. (a through l) Global plasmapause snapshots. Black dots are EUV boundary locations. Solid colored lines are corresponding simulated plasmapause curves. In 0432–0757 UT snapshots, LANL MPA in situ data from Figure 4b are represented: the yellow bullseye is the location of the LANL 1994-084 ("L4") satellite, and gray portions of geosynchronous orbit give locations where L4 observed ion density above 10 cm^{-3}. (m) Summary plot of PTP simulation output, same format as Figure 2m. (n) Solar wind E-field ϵ_{SW}, identical to Figure 2n.

40-term Fourier expansion, plotted in purple in Figure 8a. The Fourier expansion agrees with the diffuse band of EUV boundary points to within 0.2–0.4 L. In the range 1200–2100 MLT where no EUV plasmapause data were obtained, direct assessment of the accuracy of the Fourier expansion is not possible. Output from later in the simulation (section 5.3) is in agreement with LANL MPA observations of the duskside edge of the plume (discussed below), suggesting that the duskside initial plasmapause is not too unrealistic.

5.3. Simulation Results

[34] In the equatorial snapshots of Figures 8a through 8l, the black dots show the EUV boundary locations and the solid colored lines plot the corresponding simulated plasmapause curves.

5.3.1. Qualitative Performance

[35] The qualitative, global performance of the PTP simulation is quite good; enhanced convection during intervals of southward IMF (negative ϵ_{SW}, Figure 8n) causes the nightside PTP plasmapause to move inward, and the dayside to move outward and form a broad plume (Figures 8g and 8h). The plume narrows for several hours (Figures 8i and 8j) and then rotates and wraps around the main plasmasphere when convection decreases (Figures 8k and 8l).

[36] The EUV imager did not observe the duskside plasmapause between 1200 and 2100 MLT, but in section 3.3 we asserted that during 0635–0757 UT the unseen MLT sector contained a plume. The PTP simulation indeed shows a plume filling the dayside during this time (Figures 8g and 8h) and where EUV data are available, the PTP plasmapause agrees well with that of EUV, so the model plume is not inconsistent with the EUV images. Moreover, the simulated plume agrees with the geosynchronous (in situ) observations of Figure 4b. In Figures 8e through 8h, the location of the LANL 1994-084 ("L4") satellite is indicated as a yellow bullseye, and portions of the L4 orbit where dense (>10 cm^{-3}) plasma was observed are colored gray. In the simulation, the dayside plasmapause was pulled sunward so that by 0453 UT (Figure 8f) it was beginning to cross geosynchronous orbit, west of L4's location; shortly afterward at 0520 UT, the virtual (simulated) L4 crossed into the simulated dayside plume. So when the real L4 satellite entered dense plasma at 0524 UT (Figure 4b), it was probably

not crossing the western edge of a preexisting plume but rather seeing a developing plume pass by.

[37] In the PTP model the location of the duskside edge of the plume was relatively stable during the prolonged (steady) convection of 0600–0900 UT. At geosynchronous orbit, the model plume edge varied only between 1500 and 1520 MLT during this time interval; e.g., compare the blue curves of Figures 8g and 8h in the range 1500–2100 MLT. The LANL data of Figure 4 agree with the model's prediction for the dusk edge of the plume; L4 crossed into low-density plasma at 0850 UT and 1540 MLT, and the MLT of this crossing point (as given by the eastern edge of the gray-colored orbit in Figures 8g and 8h) agreed with PTP model predictions throughout the prior 3 UT hours. The implication is that the plume edge observed by L4 was stable throughout that time period.

[38] Both the PTP output and the LANL data suggest the presence of a trough of low-density plasma in the interior of the plume. As shown in Figure 4b, between 0640 and 0700 UT (or 1320–1345 MLT), L4 measured an interval of reduced density (10 cm^{-3}) relative to the surrounding plume plasma (above 25 cm^{-3}). The LANL density profile is what might be expected if L4 passed through a double plume, with duskside and dawnside portions separated by the trough [*Goldstein and Sandel*, 2005]. The PTP curve at 0635 UT (Figure 8g) contains the hint of a double plume, bifurcated by a local inward boundary deformation (the feature labeled "S") just sunward of L4. In the PTP simulation (which in effect models only a single density contour), the feature "S" represents a region of lower density in that MLT sector, consistent with the low-density trough in LANL data. The PTP double plume resulted from sunward elongation of a mild duskside bulge and shallow afternoon-sector indentation (labeled "B" and "S," respectively, in Figures 8e and 8f). The bulge B became the duskward branch of the plume, and the shallow indentation S became the trough.

[39] The model results support the interpretation that the postdawn dayside EUV boundary is actually the LST rather than a distinct (i.e., steep) density gradient. For example, in the 0453 UT snapshot (Figure 8f), the dayside PTP boundary is well sunward of the EUV boundary, but EUV may not have been able to image low enough density to observe the actual outer edge of the plasmaspheric density region. This interpretation is bolstered by the apparent agreement between the dayside PTP plasmapause and the LANL data after 0524 UT.

[40] Available geosynchronous data agree reasonably well with the plasmapause simulation on a global scale. To represent the LANL spacecraft (1994-084, 1991-080, and LANL-01A), virtual satellites were flown through the simulation, and the locations where they crossed plume edges were recorded. These simulated plume edge crossings are indicated by gray dotted vertical lines in Figure 4b (1994-084) and Figure 5d (LANL-01A). It can be seen that the simulated plume edges encompass most of the densest portions of the observed plume (0520–0820 UT in Figure 4b and 1120–1410 UT in Figure 5d), consistent with the fact that the simulated plasmapause represents the outermost boundary of plasma visible to EUV, i.e., density above the nominal EUV threshold (about 40 cm^{-3}). The virtual satellite representing 1991-080 (Figure 5b) did not encounter a plume edge, but this is again consistent with the fact that 1991-080 observed plasma density well below the EUV threshold and outside the main plume structure, and this low-density plasma is not represented by the simulation. While it is encouraging that the coarse global plasmapause shape is being captured by the model, close examination of the data highlights the inability of our approach to capture (1) the dynamics of low-density plasma and (2) the fine-scale density structure contained within the plume.

5.3.2. Quantitative Performance

[41] The quantitative performance of the model in the midnight-to-dawn MLT sector is shown in Figure 9. The blue points are the differences between the PTP-predicted and EUV-observed plasmapause L, binned by MLT (bin size 0.15 MLT hours); the maximum (minimum) magnitude of ΔL is 0.7 (1×10^{-4}). The thick black line gives the per-snapshot average error (see figure caption), $0.48L$ or less. The overall average error (red lines) is $0.24L$.

[42] The EUV plasmapause evolution (black points in Figure 8) bears evidence of a known predawn concentration of penetration E-field during both undershielding and overshielding [*Fejer and Scherliess*, 1995]. During undershielding (in which shielding is too weak to completely cancel convection), sunward flows are strongest in the postmidnight sector [*Goldstein and Sandel*, 2005], causing an indentation of the midnight-to-dawn plasmapause such as found in Figure 8b. On the other hand, predawn concentration of antisunward flows due to overshielding (in which a residual shielding E-field follows a decrease in convection) can create a predawn shoulder-like bulge of the plasmapause [*Goldstein et al.*, 2002], such as happened during 1859–2224 UT on 22 April (Figures 8i and 8j) and 1000–1200 UT on 23 April (see Figure 8m), both intervals of decreasing convection. As noted earlier (see discussion of equation (1)), the Volland-Stern convection potential approximates shielding as an MLT- and time-independent distortion of flow streamlines. This approximation ignores the spatial and temporal dependences of shielding, and so in the simulation the predawn sunward flows are too weak during times of enhanced convection and too strong during times of reduced convection. Thus in Figure 9 the predawn error in the PTP model plasmapause is generally positive during strong convection (i.e., $L_{PTP} > L_{EUV}$ before 0800 UT) and negative during decreasing convection strength (i.e., $L_{PTP} < L_{EUV}$ after 1300 UT). The most striking example of this type of disagreement is the failure of the model to reproduce the predawn shoulder of 22 April, 2224 UT (Figure 8j).

[43] As discussed in section 3.3, LANL observations contain a steep increase with MLT of the sunward flow speed, perhaps due to SAPS. In Figure 4a, the thick gray line plots the flow-speed profile obtained from the PTP simulation output by a virtual LANL satellite. In the simulated profile the observed steep rise versus MLT is not truly captured so that the duskside simulated flows are too weak by a factor of about two. This disagreement is not surprising, considering that the E-field model can reproduce only the average properties of convection and not its detailed spatial/temporal behavior. In particular, the post-0730-UT SAPS flow enhancement (See section 3.3) is a dynamic change not captured by the 3-hour cadence of the *Kp*-driven SAPS model. To study the possible role of SAPS

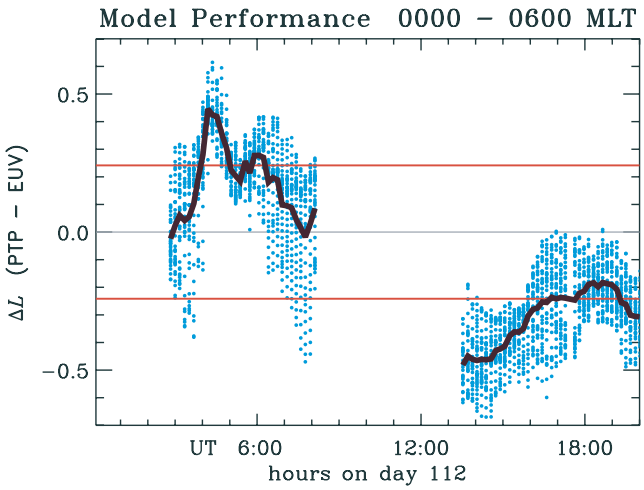

Figure 9. Quantitative assessment of PTP model performance in the midnight-to-dawn MLT sector. Horizontal axis: UT hours past midnight on day 112 (i.e., 22 April), 2001. Vertical axis: difference between model-predicted and EUV-observed plasmapause locations. All data were binned by MLT (bin size 0.15 MLT hours). The nearest-in-time PTP snapshot was compared to each EUV image; each vertical band of blue points represents one image/snapshot. The thick black line is the mean per snapshot difference between PTP and EUV plasmapause L. The overall magnitude of the average error (red horizontal lines) is $0.24L$.

in the LANL-observed flow-versus-MLT profile, we ran a second version of the code with the SAPS module disabled. The dashed gray line in Figure 4a plots the simulated flows without SAPS; the SAPS model clearly provides a major contribution to the duskside flows. So although the model does not reproduce the exact flow distribution, it does suggest a strong SAPS component. In the non-SAPS simulation, the development of the bulge (''B'' in Figures 8e and 8f) into the duskside branch of the double plume (see discussion in section 5.3.1) takes about an hour longer than in the simulation with SAPS included. In the PTP simulation, the average effect of SAPS is a $\approx 0.5\ R_E$ inward displacement (relative to the non-SAPS simulation) of the dusk-to-midnight plasmapause location and this smaller plasmapause is more in agreement with available EUV data.

[44] The model performance is worst during the plume rotation phase. According to the convective model, plume rotation occurs when the corotation-convection boundary (CCB) expands and envelops the plume. Once inside the corotation zone, the plume rotates eastward until it encounters the new CCB. A radial shear in eastward flow speed causes the base of the plume (nearer to the Earth) to rotate faster, distorting the plume's shape and causing it to wrap around the main plasmasphere. The PTP simulation reproduces some aspects of plume rotation/wrapping but misses others. In Figure 8k (0805 UT on 23 April) the nightside PTP boundary (blue curve) lines up nicely with the EUV data (black dots). However, the MLT of the base of the PTP plume is about 1 MLT hour west of the EUV plume base. This disagreement worsens with time; at 1827 UT (Figure 8l) the PTP plume is extremely narrow, just a filamentary structure flush with the CCB. The EUV plume at this time (which occupies the midnight-to-dawn MLT sector in Figure 8l) was about 2.5 R_E wide at its broadest extent (about 0300 MLT). However, as in the earlier snapshot of Figure 8k, the simulated CCB outer boundary of Figure 8l agrees with the EUV plume outer edge at that time. This comparison between the PTP and EUV rotating/wrapping plumes suggests that the CCB location is being properly modeled but that the dynamics within the CCB are not. Previous studies have suggested that simple corotation and a global convection field are inadequate to capture effects such as subcorotation [*Burch et al.*, 2004], small-scale flow eddies [*Goldstein and Sandel*, 2005], and plasma instabilities [*Lemaire and Gringauz*, 1998].

[45] This point is echoed in the comparison between Figures 2m and 8m. The PTP model L curves (Figure 8m) are roughly correct, following the EUV L curves (Figure 2m) to within about $0.7L$. However, the subglobal (i.e., $<0.7L$) scale variations in the EUV curves are not captured by the model.

[46] Figure 7c plots the model azimuthal E-field E_φ, obtained along the same plasmapause locations as the EUV E-field of Figure 7b. The three curves show the total model E_φ (black line) and the separate contributions from DMR (blue) and SAPS (red). In the PTP model the total comprises 77% from DMR and 23% from SAPS; these proportions are consistent with the relative contributions mentioned in section 5.1.1. The total E-field, at most about 9–10% of ϵ_{SW} (Figure 7b) is slightly weaker than that inferred from EUV data (which came to about 13% of ϵ_{SW}). This indicates that in the real inner magnetosphere during this time period, shielding was not as effective as it is in the Volland-Stern model.

6. Subjectivity in EUV Plasmapause L

[47] The EUV boundary locations for this event were manually extracted with the aid of a graphical program controlled by a computer mouse. In this section we quantify the subjective uncertainty in the plasmapause L. Three of the authors of the paper (JG, BRS, and WTF) participated in a ministudy in which they performed plasmapause extractions from selected images from throughout the day on 22 April 2001. The results are presented in Figure 10. Each plot of Figures 10a through 10r contains plasmapause L versus MLT from a single EUV image (UT of image indicated in the legend). The largest subjective errors are found either in regions partially obscured by the Earth's shadow (e.g., 2100–2300 MLT in Figure 10h) or where the plasmasphere in a particular EUV image possessed no steep, well-defined outer density gradient (e.g., 0300 UT, Figure 10b).

[48] The bottom three plots show all the plasmapause L values from the ministudy, in L_{author}-versus-L_{author} format. All three combinations of authors are shown: JG versus BRS, JG versus WTF, and BRS versus WTF. The blue lines show the mean difference from perfect agreement (for each plot). The maximum mean difference between two different plasmapause determinations is $0.2L$, which we take as the subjective uncertainty in the manually extracted plasma-

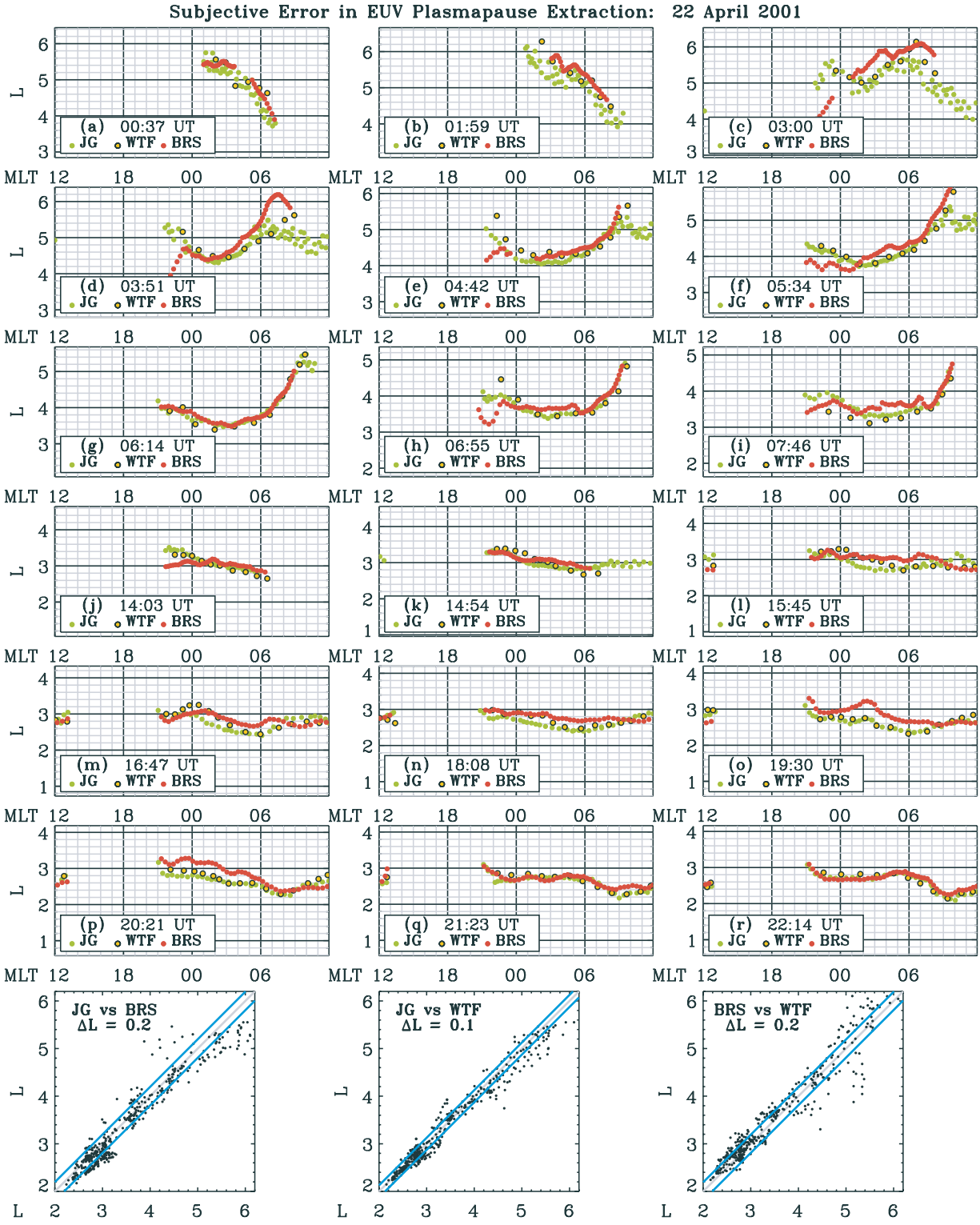

Figure 10. Subjective error in EUV plasmapause L, 22 April 2001. (a through r) Each panel shows extractions from three different authors (indicated by the legend), L plotted versus MLT. The bottom three panels show author-versus-author L plots, as described further in the text; from these bottom plots, the subjective uncertainty is $0.2L$.

pause L. This uncertainty is quite reasonable, considering the nominal EUV pixel size is $0.1R_E$.

7. Discussion and Conclusions

[49] We have shown that the global-scale dynamic behavior of the plasmapause may be quantitatively (with $0.7L$ maximum error and $0.2L$ mean error) reproduced via the use of a parametric potential electric field model that includes a crude treatment of of the SAPS effect. The model was least successful during intervals of (presumed) undershielding or overshielding, when finite-MLT-width indentations or shoulders were found in the midnight-to-dawn MLT sector, and during intervals of lessened convection, when weaker or slower effects probably play a significant role in the creation of fine-scale plasmaspheric structure. A similar model was employed by *Goldstein and Sandel* [2005], but without the SAPS model of *Goldstein et al.* [2005a], and compared only with global imaging observations to highlight the phases of plume evolution. Our study uses in situ observations as well as global images and provides a quantitative measure of the success of the model throughout the storm event.

[50] Other than the initial conditions (obtained from EUV observations), the only free parameter in the E-field model is A, the normalization constant for the Volland-Stern convection potential. This constant was specified (by trial and error) to optimize model performance, but the range of acceptable values was guided by consideration of the observed plasmapause E-field (inferred from plasmapause motion in EUV images; see section 4), and the postulate that SAPS must make some finite contribution to the dynamical evolution of the plasmapause (which is justified by previous studies [*Goldstein et al.*, 2003b]). There is ample precedent [e.g., *Maynard and Chen*, 1975] for using an available set of plasmapause observations to normalize the strength of convection, and the EUV images should not be discounted as a tool to achieve this end. A single event's worth of global plasmapauses can be equivalent (in sheer volume of data) to an entire in situ mission, and plasmapause points from different MLTs in a single global image are temporally linked (unlike in situ plasmapause locations). Nonetheless, in future simulations, the normalization constant might be better specified directly from observations (e.g., cross-polar cap potentials) rather than inferring it from plasmapause motion.

[51] The PTP model plasmapause could surely be improved. The PTP plasmapause evolution results from the collective motion of the test particles that compose it. These test particles respond only to the specified model electric field, which has contributions from corotation and two sources of convection, DMR and SAPS. The model convection E-field contains both azimuthal and radial contributions. On the nightside where the convection E-field is strongly westward, plasmapause motion results from particle motion that is both inward (from convection) and eastward (from corotation). Near the dawn flank, the dawn-to-dusk convection E-field adds to that of corotation to produce strongly eastward motion. On the duskside where corotation roughly cancels DMR-driven convection, SAPS westward flows dominate. Thus $E \times B$-drift can account for both compressional (radial) and erosional (azimuthal) motions of the particles that compose the simulated boundary, which should increase confidence in the technique whereby plasmapause motion is used to infer E-fields [*Goldstein et al.*, 2004c]. The good agreement between the PTP-simulated and EUV-observed boundaries implies that the real plasmapause might evolve similarly, as a result of the collective $E \times B$ motion of plasma elements. This hypothesis has been the basis of most (but not all) plasmaspheric models [*Lemaire and Gringauz*, 1998].

[52] In previously studied events, plasmasphere erosion began with a partial indentation of the plasmapause which then widened in MLT to gradually encompass the entire nightside [*Goldstein et al.*, 2004c, 2005b; *Goldstein and Sandel*, 2005]. Our study of the 22 April 2001 erosion event provides more evidence that this widening-indentation process is a general feature of erosion. The location of the initial indentation may be controlled by MLT concentration of the convection E-field. In the 22 April 2001 erosion, the initial indentation was in the postmidnight MLT sector, consistent with observations that show a concentration of penetration E-field in this sector [*Carpenter et al.*, 1972; *Fejer and Scherliess*, 1995]. During substorm onset, the initial indentation may occur in premidnight MLT [*Goldstein et al.*, 2005b].

[53] The 22 April plasmaspheric plume observations confirm previous studies that show distinct phases of plume evolution [*Spasojević et al.*, 2003; *Goldstein et al.*, 2004b]. In the early phase of the erosion, the plume formed as a result of the sunward motion of dayside plasma. This sunward motion is implied by the EUV images and confirmed by the in situ LANL observations of plasma density and flow. During relatively steady prolonged convection, the plume narrowed in MLT because the western plume edge migrated eastward while the duskside plume edge remained roughly stationary. The 22 April EUV images directly show only the earliest part of the plume narrowing phase, but it is clearly evident in our simulation (which agrees with available EUV plasmapause data and LANL in situ data). In both EUV images and PTP simulation snapshots, the plume rotation/wrapping phase occurred during intervals of reduced dawn-to-dusk solar wind E-field.

[54] In this paper we have shown results of a simple, parametric equatorial E-field model that includes contributions from dayside magnetopause reconnection (DMR) and the subauroral polarization stream (SAPS). Unlike the DMR contribution (i.e., the Volland-Stern model), the *Kp*-driven SAPS model potential [*Goldstein et al.*, 2005a] is relatively untested. The good agreement between our PTP simulation and the EUV plasmapauses provides some validation of the SAPS component. We have attempted to model two distinct processes (DMR and SAPS) with separately driven potential functions because in principle, SAPS flows may survive decreases in DMR-driven convection [*Anderson et al.*, 2001]. Although we do not necessarily advocate the particular potential functions used in this study, the approach (specification of separate potentials for DMR and SAPS) might be beneficial to future development of parametric E-field models.

[55] In this regard, it is worth concluding with some recommendations for enhancement of our potential functions. One particular innovation might greatly improve model performance: a better parameterization of shielding,

including both spatial inhomogeneity (especially the predawn MLT-concentration) and temporal variations. Simply varying the exponent of r in equation (1) might help, but proper treatment of overshielding would require more sophistication, perhaps following the approach of *McIlwain* [1986] or *Freeman et al.* [1993]. Although the global features of the 22 April 2001 event (plume evolution, plasmapause motion) were well-captured by the model, clearly our potentials are inadequate on spatial scales below $0.7L$, an inadequacy that persists during the entire event. PTP-EUV disagreement is especially apparent in the near-Earth zone dominated by corotation, where the model very poorly captured the inner edge of the wrapping plume.

[56] Our model study illustrates that one can get good agreement with observed plasmapause locations even if the model E-field is deficient. The model generally lacks the (unexplained) mesoscale and fine-scale features of the convection field found in numerous observations [e.g., *Wygant et al.*, 1998]. Specific to the 22 April event, the model flows are too weak in comparison to LANL observations (Figure 4a), and the model's shielding is probably too effective during the first bursts of erosion (Figure 7c). However, the best agreement between the simulated and observed plasmapauses was obtained on the nightside and duskside during strong forcing by enhanced global convection, where the smaller-scale convection fluctuations are probably less important. The plasmapause may respond on a slower timescale than the variations in the convection field, so that the integrated effect of an ''average-model'' convection E-field produces the same net result as the real field. That said, it is undoubtedly true that to use plasmapause observations to learn more about the inner magnetospheric E-field will require more careful scrutiny of the mesoscale and fine-scale plasmapause structure.

[57] **Acknowledgments.** We are grateful to N. Ness, C. Smith, D. McComas, and the ACE science center for the availability of ACE MAG and SWEPAM data. We thank the Kyoto World Data Center for Geomagnetism for providing *Dst* and the National Geophysical Data Center for providing *Kp*. This project was supported by the NASA Sun-Earth Connections Guest Investigator program under NAG5-12787 (JG), by the NASA IMAGE Mission under NAS5-96020 (JG, BRS, WTF), by the U.S. Department of Energy (MFT), and by NASA grant NAG5-9297 (MRH). Both peer reviewers have our gratitude for expert and constructive suggestions that significantly improved the paper.

[58] Arthur Richmond thanks the reviewers for their assistance in evaluating this paper.

References

Anderson, P. C., D. L. Carpenter, K. Tsuruda, T. Mukai, and F. J. Rich (2001), Multisatellite observations of rapid subauroral ion drifts (SAID), *J. Geophys. Res.*, *106*, 29,585.

Burch, J. L., J. Goldstein, and B. R. Sandel (2004), Cause of plasmasphere corotation lag, *Geophys. Res. Lett.*, *31*, L05802, doi:10.1029/2003GL019164.

Burke, W. J., et al. (1998), Electrodynamics of the inner magnetosphere observed in the dusk sector by CRRES and DMSP during the magnetic storm of June 4–6, 1991, *J. Geophys. Res.*, *103*, 29,399.

Carpenter, D. L. (1995), Earth's plasmasphere awaits rediscovery, *Eos Trans. AGU*, *76*, 89.

Carpenter, D. L., and J. Lemaire (1997), Erosion and recovery of the plasmasphere in the plasmapause region, *Space Sci. Rev.*, *80*, 153.

Carpenter, D. L., K. Stone, J. C. Siren, and T. L. Crystal (1972), Magnetospheric electric fields deduced from drifting whistler paths, *J. Geophys. Res.*, *77*, 2819.

Carpenter, D. L., B. L. Giles, C. R. Chappell, P. M. E. Decreau, R. R. Anderson, A. M. Persoon, A. J. Smith, Y. Corcuff, and P. Canu (1993), Plasmasphere dynamics in the dusk-side bulge region: A new look at an old topic, *J. Geophys. Res.*, *98*, 19,243.

Chen, A. J., and R. A. Wolf (1972), Effects on the plasmasphere of a time-varying convection electric field, *Planet. Space Sci.*, *20*, 483.

Chen, A. J., J. M. Grebowsky, and H. A. Taylor Jr. (1975), Dynamics of midlatitude light ion trough and plasma tails, *J. Geophys. Res.*, *80*, 968.

Dungey, J. W. (1961), Interplanetary magnetic field and the auroral zones, *Phys. Rev. Lett.*, *6*, 47.

Elphic, R. C., L. A. Weiss, M. F. Thomsen, D. J. McComas, and M. B. Moldwin (1996), Evolution of plasmaspheric ions at geosynchronous orbit during times of high geomagnetic activity, *Geophys. Res. Lett.*, *23*, 2189.

Fejer, B. G., and L. Scherliess (1995), Time dependent response of equatorial ionospheric electric fields in magnetospheric disturbances, *Geophys. Res. Lett.*, *22*, 851.

Fok, M., R. A. Wolf, R. W. Spiro, and T. E. Moore (2001), Comprehensive computational model of Earth's ring current, *J. Geophys. Res.*, *106*, 8417.

Foster, J. C., and W. J. Burke (2002), SAPS: A new categorization for subauroral electric fields, *Eos Trans. AGU*, *83*, 393.

Foster, J. C., and H. B. Vo (2002), Average characteristics and activity dependence of the subauroral polarization stream, *J. Geophys. Res.*, *107*(A12), 1475, doi:10.1029/2002JA009409.

Foster, J. C., P. J. Erickson, A. J. Coster, and J. Goldstein (2002), Ionospheric signatures of plasmaspheric tails, *Geophys. Res. Lett.*, *29*(13), 1623, doi:10.1029/2002GL015067.

Freeman, J. W., R. A. Wolf, R. W. Spiro, G.-H. Voigt, B. A. Hausman, B. A. Bales, R. V. Hilmer, A. Nagai, and R. L. Lambour (1993), Magnetospheric Specification Model development code and documentation, *Rep. for USAF Contract F19628-90-K-0012*, Rice Univ., Houston, Tex.

Goldstein, J., and B. R. Sandel (2005), The global pattern of evolution of plasmaspheric drainage plumes, in *Inner Magnetosphere Interactions: New Perspectives from Imaging*, vol. 159, edited by J. L. Burch, M. Schulz, and H. Spence, p. 1, AGU, Washington, D. C.

Goldstein, J., R. W. Spiro, P. H. Reiff, R. A. Wolf, B. R. Sandel, J. W. Freeman, and R. L. Lambour (2002), IMF-driven overshielding electric field and the origin of the plasmaspheric shoulder of May 24, 2000, *Geophys. Res. Lett.*, *29*(16), 1819, doi:10.1029/2001GL014534.

Goldstein, J., B. R. Sandel, W. T. Forrester, and P. H. Reiff (2003a), IMF-driven plasmasphere erosion of 10 July 2000, *Geophys. Res. Lett.*, *30*(3), 1146, doi:10.1029/2002GL016478.

Goldstein, J., B. R. Sandel, P. H. Reiff, and M. R. Hairston (2003b), Control of plasmaspheric dynamics by both convection and sub-auroral polarization stream, *Geophys. Res. Lett.*, *30*(24), 2243, doi:10.1029/2003GL018390.

Goldstein, J., M. Spasojević, P. H. Reiff, B. R. Sandel, W. T. Forrester, D. L. Gallagher, and B. W. Reinisch (2003c), Identifying the plasmapause in IMAGE EUV data using IMAGE RPI in situ steep density gradients, *J. Geophys. Res.*, *108*(A4), 1147, doi:10.1029/2002JA009475.

Goldstein, J., R. W. Spiro, B. R. Sandel, R. A. Wolf, S.-Y. Su, and P. H. Reiff (2003d), Overshielding event of 28–29 July 2000, *Geophys. Res. Lett.*, *30*(8), 1421, doi:10.1029/2002GL016644.

Goldstein, J., B. R. Sandel, M. R. Hairston, and S. B. Mende (2004a), Plasmapause undulation of 17 April 2002, *Geophys. Res. Lett.*, *31*, L15801, doi:10.1029/2004GL019959.

Goldstein, J., B. R. Sandel, M. F. Thomsen, M. Spasojević, and P. H. Reiff (2004b), Simultaneous remote-sensing and in situ observations of plasmaspheric drainage plumes, *J. Geophys. Res.*, *109*, A03202, doi:10.1029/2003JA010281.

Goldstein, J., R. A. Wolf, B. R. Sandel, and P. H. Reiff (2004c), Electric fields deduced from plasmapause motion in IMAGE EUV images, *Geophys. Res. Lett.*, *31*, L01801, doi:10.1029/2003GL018797.

Goldstein, J., J. L. Burch, and B. R. Sandel (2005a), Magnetospheric model of subauroral polarization stream, *J. Geophys. Res.*, *110*, A09222, doi:10.1029/2005JA011135.

Goldstein, J., J. L. Burch, B. R. Sandel, S. B. Mende, P. C:son Brandt, and M. R. Hairston (2005b), Coupled response of the inner magnetosphere and ionosphere on 17 April 2002, *J. Geophys. Res.*, *110*, A03205, doi:10.1029/2004JA010712.

Grebowsky, J. M. (1970), Model study of plasmapause motion, *J. Geophys. Res.*, *75*, 4329.

Higel, B., and L. Wu (1984), Electron density and plasmapause characteristics at 6.6 RE: A statistical study of the GEOS 2 relaxation sounder data, *J. Geophys. Res.*, *89*, 1583.

Jaggi, R. K., and R. A. Wolf (1973), Self-consistent calculation of the motion of a sheet of ions in the magnetosphere, *J. Geophys. Res.*, *78*, 2852.

Kelley, M. C., B. G. Fejer, and C. A. Gonzales (1979), An explanation for anomalous ionospheric electric fields associated with a northward turning of the interplanetary magnetic field, *Geophys. Res. Lett.*, *6*, 301.

Korth, H., M. F. Thomsen, J. E. Borovsky, and D. J. McComas (1999), Plasma sheet access to geosynchronous orbit, *J. Geophys. Res.*, *104*, 25,407.

Lambour, R. L., L. A. Weiss, R. C. Elphic, and M. F. Thomsen (1997), Global modeling of the plasmasphere following storm sudden commencements, *J. Geophys. Res.*, *102*, 24,351.

Lemaire, J. F., and K. I. Gringauz (1998), *The Earth's Plasmasphere*, Cambridge Univ. Press, New York.

Liemohn, M. W., A. J. Ridley, D. L. Gallagher, D. M. Ober, and J. U. Kozyra (2004), Dependence of plasmaspheric morphology on the electric field description during the recovery phase of the 17 April 2002 magnetic storm, *J. Geophys. Res.*, *109*, A03209, doi:10.1029/2003JA010304.

Maynard, N. C., and A. J. Chen (1975), Isolated cold plasma regions: Observations and their relation to possible production mechanisms, *J. Geophys. Res.*, *80*, 1009.

McComas, D. J., S. J. Bame, B. L. Barraclough, J. R. Donart, R. C. Elphic, J. T. Gosling, M. B. Moldwin, K. R. Moore, and M. F. Thomsen (1993), Magnetospheric Plasma Analyzer (MPA): Initial three-spacecraft observations from geosynchronous orbit, *J. Geophys. Res.*, *98*, 13,453.

McIlwain, C. E. (1986), A K_p dependent equatorial electric field model, *Adv. Space Res.*, *6*, 187.

Moldwin, M. B., M. F. Thomsen, S. J. Bame, D. J. McComas, and K. R. Moore (1994), An examination of the structure and dynamics of the outer plasmasphere using multiple geosynchronous satellites, *J. Geophys. Res.*, *99*, 11,475.

Roelof, E. C., and A. J. Skinner (2000), Extraction of ion distributions from magnetospheric ENA and EUV images, *Space Sci. Rev.*, *91*, 437.

Sandel, B. R., R. A. King, W. T. Forrester, D. L. Gallagher, A. L. Broadfoot, and C. C. Curtis (2001), Initial results from the IMAGE extreme ultraviolet imager, *Geophys. Res. Lett.*, *28*, 1439.

Senior, C., and M. Blanc (1984), On the control of magnetospheric convection by the spatial distribution of ionospheric conductivities, *J. Geophys. Res.*, *89*, 261.

Spasojević, M., J. Goldstein, D. L. Carpenter, U. S. Inan, B. R. Sandel, M. B. Moldwin, and B. W. Reinisch (2003), Global response of the plasmasphere to a geomagnetic disturbance, *J. Geophys. Res.*, *108*(A9), 1340, doi:10.1029/2003JA009987.

Spiro, R. W., M. Harel, R. A. Wolf, and P. H. Reiff (1981), Quantitative simulation of a magnetospheric substorm: 3. Plasmaspheric electric fields and evolution of the plasmapause, *J. Geophys. Res.*, *86*, 2261.

Stern, D. P. (1975), The motion of a proton in the equatorial magnetosphere, *J. Geophys. Res.*, *80*, 595.

Stone, E. C., A. M. Frandsen, R. A. Mewaldt, E. R. Christian, D. Margolies, J. F. Ormes, and F. Snow (1998), The Advanced Composition Explorer, *Space Sci. Rev.*, *86*, 1.

Volland, H. (1973), Semiempirical model of large-scale magnetospheric electric fields, *J. Geophys. Res.*, *78*, 171.

Weiss, L. A., R. L. Lambour, R. C. Elphic, and M. F. Thomsen (1997), Study of plasmaspheric evolution using geosynchronous observations and global modeling, *Geophys. Res. Lett.*, *24*, 599.

Wygant, J. R., D. E. Rowland, H. J. Singer, M. Temerin, F. Mozer, and M. K. Hudson (1998), Experimental evidence on the role of the large spatial scale electric field in creating the ring current, *J. Geophys. Res.*, *103*, 29,527.

J. Goldstein, Southwest Research Institute, 6220 Culebra Road, San Antonio, TX 78228, USA. (jgoldstein@swri.edu)

M. R. Hairston, Center for Space Sciences, University of Texas at Dallas, P.O. Box 830688 FO22, Richardson, TX 75083, USA.

B. R. Sandel and W. T. Forrester, Lunar and Planetary Laboratory, University of Arizona, 1541 E. University Blvd., Tucson, AZ 85721, USA.

M. F. Thomsen, Los Alamos National Laboratory, MS D466, Los Alamos, NM 87545, USA.